Journal of Science and Technology – Engineering and Technology for Sustainable Development
Volume 36, Issue 4, October 2026, 064–069

Evaluation and Analyzing of Air Drying Distribution in Chamber with Tuned Relative Vertical Position of Frames

Trung Nguyen Duc[1,*], Giang Nguyen Truong[1], Thao Nguyen Thi[2], Hieu Nguyen Trung[3], Anh Nguyen Thi Ngoc[2], Cuong Le Ngoc[1], Huong Pham Thanh[1], Thuy Phan Minh[1], Hoang Nguyen Ngoc[1]

[1]*School of Chemistry and Life Sciences, Hanoi University of Science and Technology, Ha Noi, Vietnam*
[2]*Green Technology and Digital Transformation Co., Ltd, Ha Noi, Vietnam*
[3]*School of Material Sciences, Hanoi University of Science and Technology, Ha Noi, Vietnam*
[*]*Corresponding author: trung.nguyenduc@hust.edu.vn*

Abstract

Drying efficiency strongly depends on the uniformity of airflow distribution within the drying chamber. In the study, two-dimensional Computational Fluid Dynamics (CFD) simulations were employed to analyze airflow behavior in a multi-tray drying chamber with six geometric configurations characterized by different frame steps (S). The results reveal that airflow uniformity decreases with chamber height, with pronounced instabilities observed at the upper frames. The value of S was found to play a critical role in airflow distribution. The most popular design of case I with zero-step (baseline) exhibited the poorest performance, with relative standard deviation (RSD) exceeding 55.6% and the largest inhomogeneity with max to min discrepancy (M2M up to 12.5), indicating strong airflow irregularity. In contrast, case V with the tuned vertical step of frame at 30 mm demonstrated the best performance, with RSD as low as 18.7–28.1% and minimal M2M differences, reflecting highly uniform airflow across the tray surfaces. The bigger absolute value of step gave better performance than the smaller ones because the drying airflow tends to follow the surface of trays. Compared to previous studies, these findings underscore the importance of evaluating airflow directly at the tray surfaces rather than solely at the chamber scale. Overall, the study offers practical guidance for optimizing tray arrangement and frame step design to improve airflow uniformity, thereby enhancing drying performance and product quality.

Keywords: Airflow distribution, CFD simulation, drying air effectiveness, drying chamber, frame step, uniformity.

1. Introduction

Drying is an effective preservation method widely applied to various materials, particularly in food technology [1]. The homogeneity of moisture distribution is a key factor in determining the quality of dried products and extending their shelf life [2]. The distribution of airflow has a direct impact on the performance of drying processes. Non-uniform air distribution results in heterogeneous drying rates, product quality degradation, and energy inefficiency. The initially uneven air distribution in the drying chamber may lead to drying efficiency reduction [3]. Therefore, ensuring uniform air distribution across all trays and chamber zones has become central focus in dryer design and optimization.

Experimental research and analysis are both costly and time intensive [4]. Consequently, Computational Fluid Dynamics (CFD) simulations have been increasingly employed to enhance chamber drying due to their efficiency in evaluating airflow distribution and their cost-effectiveness [3]. Numerous studies have concentrated on evaluating and optimizing dryer designs to ensure a more uniform airflow distribution within the drying chamber [5-7]. Modifying the tray arrangement improves the uniformity of airflow within the drying chamber [5]. The integration of a mesh-type air inlet in the drying chamber produced a concentrated airflow directly over the sample surface, compared with a chamber without a mesh air inlet [6]. Improving the air distribution system within the drying chamber enhances drying efficiency [7].

The effectiveness of airflow interactions in regions directly impacting the material surface has not been evaluated, with prior research focusing instead on the overall uniformity of airflow distribution throughout the drying chamber [5-7]. Higher air velocities enhance airflow-material interaction, improving drying efficiency [6]. This study employs 2D CFD simulations to investigate the effects of varying tray heights on airflow within the drying chamber. Significant variations in air velocity and pressure occur only along the horizontal and vertical directions of the drying chamber whose length and height are so big that the 3D – air distribution can be approximately evaluated in 2D – plane. In addition, it introduces an approximate method to evaluate airflow distribution near material surfaces, assuming a uniformly distributed inlet across the dryer geometry.

p-ISSN 3093-3242
e-ISSN 3093-3579
https://doi.org/10.51316/jst.193.etsd.2026.36.4.8
Received: Oct 21, 2025; Revised: Nov 26, 2025;
Accepted: Dec 25, 2025; Online: Jun 22, 2026

2. Materials and Methods

2.1. Characteristics of Dryer Geometry

The drying system is composed of three frames (or three trolleys). Each frame accommodating 15 trays. Each tray which contains materials, has dimensions of 600mm × 600mm × 30 mm ($L \times W \times H$). The *Ox, Oy*, and *Oz* axes respectively denote the length (a), width (b), and height (c) directions of the drying equipment.

The drying airflow from the calorifier enters and pass-through inlet duct, drying chamber and outlet duct with the same width of airgap which is equal to width of drying equipment ("b" along *Oy* axis in the Fig. 1). The airflow travelling length in this study is much bigger enough than the airgap "b" so the airflow can be considered uniform at *Oy* axis.

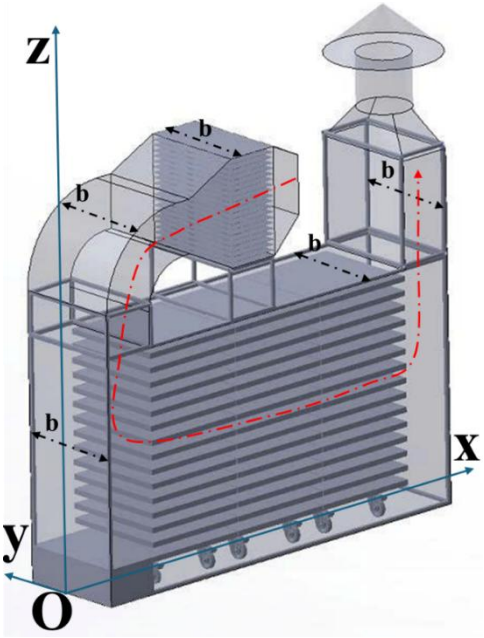


Fig. 1. 3D-visualization of chamber drying

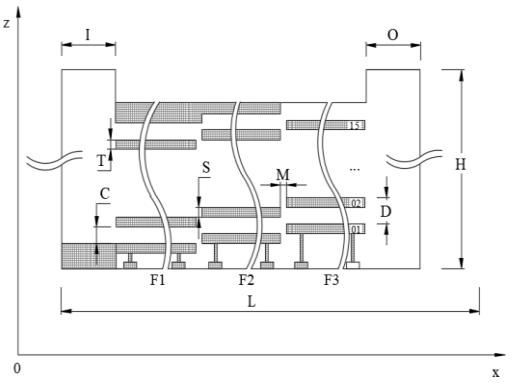


Fig. 2. 2D-geometry dimensions of chamber drying

The airflow in the drying chamber can be assessed on Oxz at Fig 2. Many previous studies also applied 2D/3D approximation method because of similar result of distribution prediction [8, 9].

The geometric dimensions in Fig. 2. of the system are summarized in Table 1. Both cases whose frame steps are equal to +40 (mm) or –40 (mm) are overlapped as shown in Fig. 3. Case VI represents an identical symmetric topology and a special condition in which S is equal to the half of distance of two continuous trays ($D/2$ = 40 mm). The airgap size at both of lower and upper part of each tray are also equal (15 mm). The variation of absolute value of S has to be upper limited at 40 (mm) because of the topology repetition caused by the geometrical period (D).

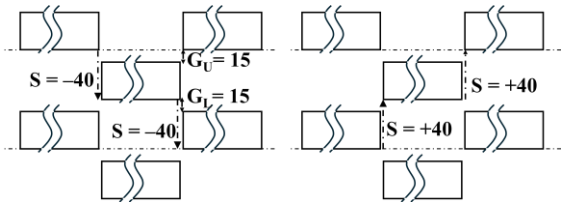


Fig. 2. The overlapping: $S = \pm 40$

Table. 1. Geometric dimensions

Symbol	Description	Value (mm)
C	Air spacing from the top of m^{th} tray to the bottom of $(m+1)^{th}$ tray of same frame	50
D	Distance from the bottom of m^{th} tray to the bottom of $(m+1)^{th}$ tray of same frame	80
H	Chamber height	1495
I	Inlet width	300
O	Outlet width	300
S	Frames step	Variable value
T	Thickness of tray and material	30
L	Chamber length	2420
M	Distance from frame to frame	6

Table. 2. Assessed value of *S*

Case	I	II	III	IV	V	VI
S	0	+15	−15	+30	−30	±40

This study assesses the drying air distribution at each tray due to the variation of S in the Table 2 via statistical criterions of objective function in next parts.

2.2. Estimation Function of Drying Air Effectiveness

The study proposes an approximate method for velocity distribution using a height-based weighting function. For the same value of momentum, the drying air part which are nearer to the tray establishes more effective to material dehumidification. Therefore, the vertical weighting function (w) which describes the relative vertical elevation of each element, needs to be multiplied to momentum (P_i) of each element. The total momentum of air flow affects directly to collision and contact between drying air and drying material which enhances moisture removal.

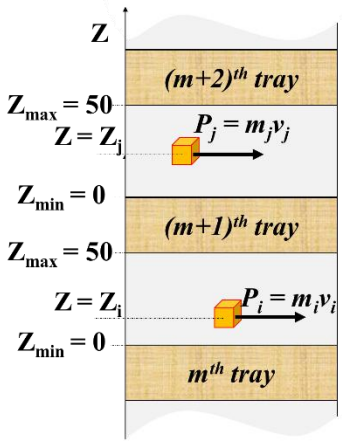


Fig. 3. Air spacing

The objective function can be mathematically expressed with vertical weighting coefficient (w):

$$J = \sum_{i=1}^{n} wP_i = \sum_{i=1}^{n} w(m_i v_i) \quad (1)$$

The number of differentially meshed elements in air gap for each tray is noted "n" in (1) Since air density of drying air ρ varies slightly at operational temperature range which is from about 60 ºC to about 70 ºC, the above equation can be converted to:

$$J = \sum_{i=1}^{n} w(m_i v_i) = \rho \sum_{i=1}^{n} w\, V_i v_i \quad (2)$$

For two-dimensional simulation, the basic elements are not volume difference V_i, are area difference A_i because of same width of chamber (b). The equation (2) can be rewritten:

$$J = \rho \sum_{i=1}^{n} w(bA_i)v_i = \rho b \sum_{i=1}^{n} \mathrm{w}\,(A_i v_i) \quad (3)$$

The objective function (3) can be rewritten:

$$K = \frac{\mathrm{J}}{\rho d} = \sum_{i=1}^{n} wA_i v_i \quad (4)$$

The weighting function led to be smaller at higher relative vertical elevations. To synchronize the calculation, the value of the proposed weighting function (w) at the surface of each tray is normalized to the unit interval 0–1. Two typical weighting function are mathematically expressed in linear type and exponential type:

$$\mathrm{w}_1 = g(z_\mathrm{i}) = 1 - \frac{z_\mathrm{i}}{z_\mathrm{max}} \quad (5)$$

$$\mathrm{w}_2 = f(z_\mathrm{i}) = \mathrm{e}^{-\alpha\frac{z_\mathrm{i}}{z_\mathrm{max}}} \quad (6)$$

The sensitivity of weighting function at one tray calculation is visualized graphically in unit window; as depicted in Fig. 4.

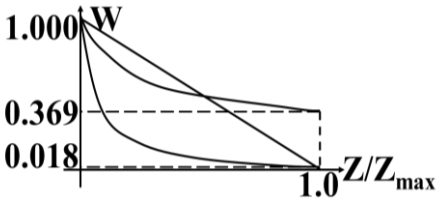


Fig. 4. Graph of numerous weighting functions

The bigger value of α at selected w_2 makes the estimation of objective function more sensitive. In this study, the weighting function (w) is calculated due to vertical position of meshed elements z with the value of α which is equal to 3 because the ratio of the width of the airgap to the length of tray is rather small.

2.3. Evaluation Criteria of Drying Air Distribution

The average weighted function value of a frame (A_K) and standard deviation (STD) of K of the trays at the same frame or at the whole chamber are calculated to estimate the relative standard deviation (RSD in %) which expresses the correlative distribution of drying air effectiveness to each tray exactly because of the independence from the amplitude of air velocity.

The average value (A_K) of K is expressed by the following formula:

$$A_K = \frac{1}{N}\sum_{m=1}^{N} K_m \quad (7)$$

where N is the number of drying trays, K_m is weighted function value of m^{th} tray in the same frame.

The STD is expressed by the following formula:

$$STD = \sqrt{\frac{1}{N}\sum_{m=1}^{N}(K_m - A_K)^2} \quad (8)$$

The RSD is expressed as:

$$SRD = \frac{STD}{A_K}100 \quad (9)$$

The ratio of the maximum of K (K_{max}) to the minimum of K (K_{min}) in the whole chamber (Ch) or in one certain frame ($F1$, $F2$, $F3$), is formulated as:

$$M2M = \frac{K_{max}}{K_{min}} \quad (10)$$

The $M2M$ factor can be called maximum to minimum ratio. RD and $M2M$ are selected criterions to evaluate the distribution of drying air effectiveness.

2.4. System Modelling and k–ω Turbulence Model

The governing equations of fluid motion consist of the continuity, momentum Navier–Stokes, and energy equations. The continuity equation ensures mass conservation:

$$\frac{\partial \rho}{\partial t} + \nabla(\rho u) = 0 \tag{11}$$

while the momentum conservation is formulated as:

$$\rho\left(\frac{\partial u}{\partial t} + (u\nabla)u\right) = -\nabla p + \mu\nabla^2 u + \rho f \tag{12}$$

where u is the velocity vector, p is the pressure, μ is the dynamic viscosity, and f is the body force per unit mass.

The Navier–Stokes equations are nonlinear partial differential equations (PDEs) that rarely have analytical solutions in practical applications. Therefore, CFD overcomes this limitation by numerically approximating solutions, facilitating in-depth analysis of complex flow phenomena.

In CFD, the finite volume method (FVM) is widely used to discretize and solve the governing equations, ensuring the conservation of mass, momentum, and energy. The turbulence kinetic energy (*k)* is expressed as the formula [10]:

$$\frac{\partial}{\partial t}(\rho k) + \frac{\partial}{\partial x_j}(\rho k u_i) = \frac{\partial}{\partial x_j}\left(\Gamma_k \frac{\partial k}{\partial x_j}\right) + G_k - Y_k + S_k + G_b \tag{13}$$

The specific dissipation rate ω is obtained from the following equations:

$$\frac{\partial}{\partial t}(\rho \omega) + \frac{\partial}{\partial x_j}(\rho \omega u_i) = \frac{\partial}{\partial x_j}\left(\Gamma_k \frac{\partial \omega}{\partial x_j}\right) + G_\omega - Y_\omega + S_\omega + G_\omega \tag{14}$$

Turbulence is typically modeled using the *k*–ω model whose formulation is particularly popular for its combination of accurate near-wall treatment and improved prediction of separated flows [10]. The *k*–ω model is widely used in tray and tunnel drying equipment, providing accurate predictions with moderate computational effort [9, 10].

2.5. Simulation Software and Meshing Method

In this study, the 2D geometric model of the drying chamber was developed in AutoCAD 2022. CFD simulations were then conducted in ANSYS Fluent V19.2 to analyze the airflow distribution inside the chamber.

ANSYS Fluent V19.2 can handle the complex computation the *k–ω* model exactly and reliably with appropriate meshing method [11, 12]. The selected size for meshing is based on the different factors: dimension of airgap region, geometry topology of solid material and hypothesis about the drying material. The quality of the mesh plays a decisive role in determining the accuracy of CFD simulations. In this study, the computational domains of the models were discretized with mesh configurations that ensure good quality metrics suitable for two-dimensional simulations. The mesh statistics and quality indicators are summarized in Table 3.

Table. 3. Mesh results

Case	Element size (mm)	Elements	Type of elements	Skewness
I	5	138825	Quad4	< 0.65
II	5	136486	Quad4	< 0.63
III	5	136519	Quad4	< 0.71
IV	5	135808	Quad4	< 0.7
V	5	135824	Quad4	< 0.58
VI	5	134331	Quad4	< 0.53

The Ansys simulation results are exported to Microsoft Excel 2019 to calculate the value of weighted objective function. The statistical criterions are also estimated directly in Microsoft Excel 2019.

3. Result and Discussion

The evaluation criteria of drying air distribution were calculated and shown in Table 4. The analysis shows clear differences in airflow uniformity depending on the vertical frame step configuration.

Among all cases, case *I* (*S* = 0) produced the poorest performance, with the *RSD* of *Ch* exceeding 55.6% and *M2M* of *Ch* discrepancies as high as 12.5. The simulation result of the most popular design indicates highly irregular airflow and huge uniformity of air drying distribution.

In contrast, case V (*S* = – 30 mm) achieved the most favorable outcome. Both the *RSD* and the *M2M* of *Ch* are the smallest among all cases, at 28.1% and 3.05, respectively. This improvement can be attributed to the tuned displacement of trays. By limiting excessive fluctuations at higher levels, the airflow was redistributed more evenly, leading to enhanced contact between drying air and material surfaces.

An important observation is the distinctive behavior of case VI (*S* = ±40 mm). Owing to its geometric symmetry, case VI provides a balanced air inlet condition. However, while the *RSD* of *Ch* in case VI are moderate at 29.3%. As a result, although case VI demonstrates better uniformity than case I, it still does not surpass the optimized arrangement in case V. Case VI shows that geometric symmetry can enhance balance but does not fully resolve competition effects at identical elevations. Case II (*S* = +15 mm) still exhibits high irregularity, with the *RSD* of *Ch* above 47%. Case III (*S* = –15mm) which shows a clear improvement; both the RSD and the *M2M* of Ch are smaller than case II at

39.8%, 3.6, respectively. Case IV (S = +30 mm) demonstrates a further enhancement, with the *RSD* of *Ch* is equal to 32.7% and the *M2M* is equal to 3.34. The results show that the bigger absolute value of step gave better performance than the smaller ones because the drying airflow tends to follow the surface of trays. Considering all six cases, the overall ranking from best to worst airflow uniformity is, respectively: case V, case VI, case IV, case III, case II, and case I.

Table. 4. The impact of vertical position tuning to the distribution of airdrying effectiveness

Case	Region	A_K (x10^{-3})	*STD* (x10^{-3})	*M2M*	*RSD* (%)
I	F1	8.80	4.44	6.47	3.4
	F2	6.37	3.45	9.19	54.1
	F3	6.16	3.33	7.79	54.0
	Ch	7.11	3.96	12.50	55.6
II	F1	8.90	3.95	3.98	42.4
	F2	6.44	2.87	4.45	44.6
	F3	6.55	2.78	4.19	42.4
	Ch	7.30	3.44	6.55	47.1
III	F1	9.01	3.07	2.70	34.1
	F2	6.02	1.89	2.38	31.4
	F3	5.91	1.98	2.42	33.5
	Ch	6.98	2.78	3.60	39.8
IV	F1	9.10	2.36	2.94	25.9
	F2	5.69	1.06	1.85	18.7
	F3	5.89	1.09	1.78	18.6
	Ch	6.90	2.25	3.34	32.7
V	F1	9.58	1.90	1.89	19.8
	F2	6.38	1.19	1.99	18.7
	F3	6.89	1.68	2.08	24.5
	Ch	7.62	2.14	3.05	28.1
VI	F1	9.41	1.93	2.51	20.5
	F2	6.66	1.36	2.04	20.5
	F3	6.66	2.05	4.66	30.6
	Ch	7.59	2.22	6.40	29.3

Fig. 5. and Fig. 6. illustrate the distribution visually for the most popular topology at case I an the most symmetric topology at case V. The most symmetric topology at case V cannot establish the most uniform distribution because evaluating objective function is created by the multiplication of momentum of each differential element with its vertical position (z) and the inlet direction of drying airflow to the chamber is reverse to the outlet one of drying airflow from the chamber.

Misha *et al.* [5] also investigated the effects of varying tray arrangements in a drying chamber model with three frames. They analyzed a planar section extracted from the 3D simulation to evaluate airflow and temperature distribution throughout the entire drying chamber. The designs surveyed include cases like case I and case VI in this study. Furthermore, they employed a specially designed drying chamber model to control and optimize airflow distribution, and the results showed that the arrangement with S equal 0 achieved the best performance among the designs.

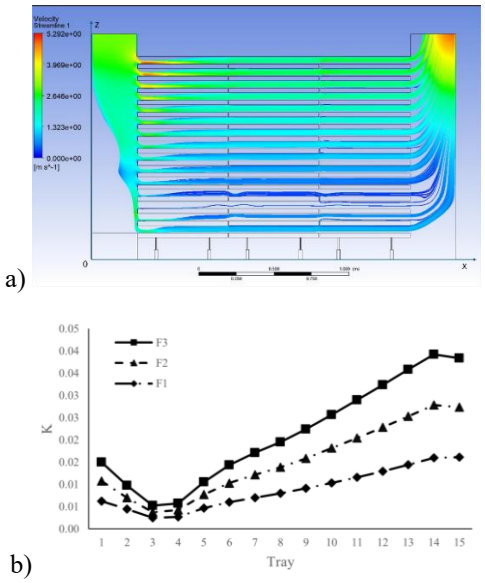


Fig. 5. a) 2D visualization of air distribution – case I, b) K–values at different trays – case I

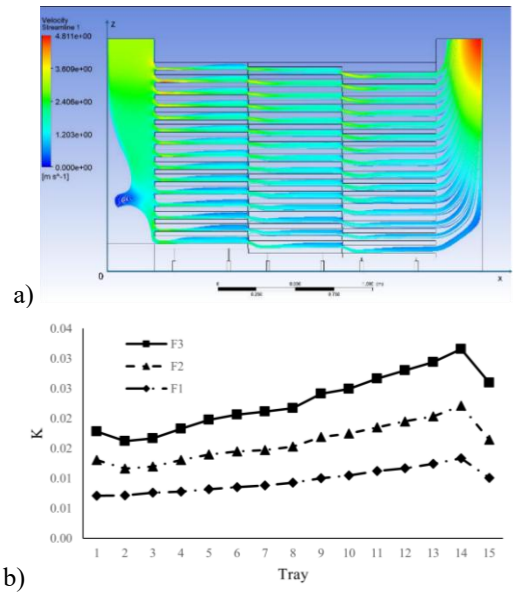


Fig. 6. a) 2D visualization of air distribution – case V, b) K–values at different trays – case V

However, the results of this study indicate that even when using a conventional drying chamber model, case VI still outperforms case I (Table 4). An issue of Misha *et al* [3] study is evaluating distribution only at the chamber scale, without considering the effectiveness of airflow directly on the tray surfaces; the airflow distribution was found to be highly concentrated in the upper trays near the inlet, which reduced the airflow reaching the lower trays and consequently diminished the drying efficiency in those regions.

4. Conclusion

This study employed CFD simulations to evaluate airflow distribution in a multi-tray drying chamber under six frame step configurations. The results clearly show that tray positioning plays a decisive role in achieving uniform airflow, which directly governs drying effectiveness.

The most popular design (case I with baseline) produced the poorest performance, with the *RSD* of *Ch* exceeding 55.6% and *M2M* up to 12.5, reflecting severe irregularities, particularly at the upper trays. This design is easiest to manufacture equipment. In contrast, Case V achieved the most uniform airflow, with the *RSD* and the *M2M* of *Ch* are only equal to 28.1% and 3.05, as follows. Case V ensures effective contact between drying air and material surfaces. Case VI (S = ± 40 mm with symmetrical topology) ranked second best, with chamber *RSD* at 29.3%, although local competition at trays of identical elevation led to a higher *M2M* of 6.40. This design is also second easiest to manufacture equipment. Cases II, III, and IV showed progressive improvement, with chamber *RSD* of 47.1%, 39.8%, and 32.7%, respectively.

As the uneven airflow patterns along the chamber height and frame length are similar across all cases in this study, the different types of drying equipment should be assessed to improve the performance via more uniform distribution of drying airflow effectiveness to drying material.

References

[1] Á. Calín-Sánchez, L. Lipan, M. Cano-Lamadrid, A. Kharaghani, K. Masztalerz, Á. A. Carbonell-Barrachina, and A. Figiel, Comparison of traditional and novel drying techniques and its effect on quality of fruits, vegetables and aromatic herbs, Foods, vol. 9, iss. 9, Sep. 2020, Art. no. 1261. https://doi.org/10.3390/foods9091261

[2] P. Schinabeck, M. Pfannemüller, S. Schlüter, and H. Kulozik, Effect of moisture distribution on the quality and storage stability of dried food products, Journal of Food Engineering, vol. 243, pp. 63–71, Sep. 2019.

[3] S. Misha, S. Mat, M. A. M. Rosli, M. H. Ruslan, K. Sopian, and E. Salleh, Simulation of air flow distribution in a tray dryer by CFD, Applied Mechanics and Materials, vol. 699, pp. 887–892, Apr. 2015.

[4] F. U. Rehman, L. Huang, E. Anderlini, and G. Thomas, Hydrodynamic modelling for a transportation system of two unmanned underwater vehicles: Semi-empirical, numerical and experimental analyses, Journal of Marine Science and Engineering, vol. 9, iss. 5, May 2021, Art. no. 500. https://doi.org/10.3390/jmse9050500

[5] S. Misha, S. Mat, M. H. Ruslan, K. Sopian, and E. Salleh, The CFD simulation of tray dryer design for kenaf core drying, Applied Mechanics and Materials, vol. 393, pp. 717–722, Sep. 2013. https://doi.org/10.4028/www.scientific.net/AMM.393.717

[6] A. Hassan, M. U. H. Joardder and A. Karim, A CFD integrated drying model for improving drying conditions in industry-scale dryers, Thermal Science and Engineering Progress, vol. 61, May 2025, Art. no. 103533. https://doi.org/10.1016/j.tsep.2025.103533

[7] D. Cebulski and P. Cyklis, Application of CFD simulation to the design of an innovative drying chamber, Energies, vol. 17, iss. 13, Jul. 2024, Art. no. 3338. https://doi.org/10.3390/en17133338

[8] N. Therdthai, W. Zhou, and T. Adamczak, Two-dimensional CFD modelling and simulation of an industrial continuous bread baking oven, Journal of Food Engineering, vol. 60, iss. 2, pp. 211–217, Nov. 2003. https://doi.org/10.1016/S0260-8774(03)00043-8

[9] M. A. R. Kavindi, K. S. P. Amaratunga, E. M. A. C. Ekanayake, A. J. Fernando, and A. M. S. K. Abesinghe, CFD simulation of airflow distribution in a heat pump-assisted deep-bed paddy dryer, Applied Engineering in Agriculture, vol. 38, no. 1, pp. 1–8, 2022. https://doi.org/10.13031/aea.14483

[10] ANSYS Inc., ANSYS Fluent Theory Guide, Release 2022 R1, Canonsburg, PA, USA, 2022.

[11] A. R. Visconcini, C. M. G. Andrade, and A. M. de S. Costa, Fluid flow simulation of industrial fixed bed mixed-flow grain dryer using k–ω SST turbulence model, International Journal of Agricultural and Biological Engineering, vol. 14, no. 2, pp. 226–230, 2021. https://doi.org/10.25165/j.ijabe.20211402.5321

[12] S. T. S. Sileshi, A. A. Hassen, and K. D. Adem, Simulation of mixed-mode solar dryer with vertical air distribution channel, Heliyon, vol. 8, no. 11, Nov. 2022, Art. no. e11898. https://doi.org/10.1016/j.heliyon.2022.e11898